Provided for non-commercial research and education use.
Not for reproduction, distribution or commercial use.

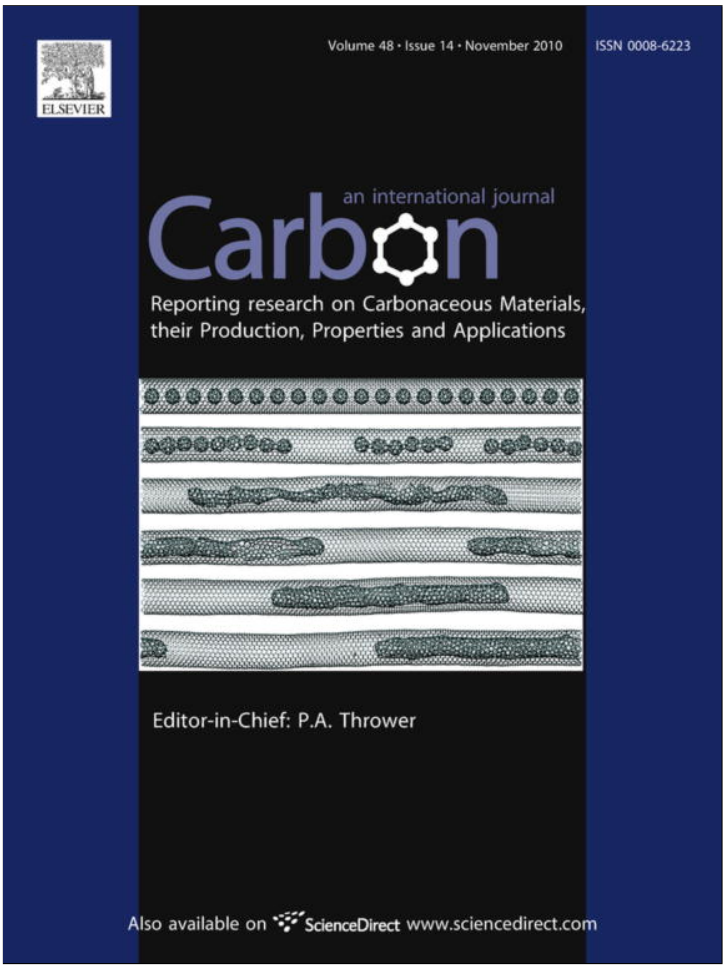

This article appeared in a journal published by Elsevier. The attached copy is furnished to the author for internal non-commercial research and education use, including for instruction at the authors institution and sharing with colleagues.

Other uses, including reproduction and distribution, or selling or licensing copies, or posting to personal, institutional or third party websites are prohibited.

In most cases authors are permitted to post their version of the article (e.g. in Word or Tex form) to their personal website or institutional repository. Authors requiring further information regarding Elsevier's archiving and manuscript policies are encouraged to visit:

http://www.elsevier.com/copyright

Author's personal copy

CARBON 48 (2010) 4042–4048

available at www.sciencedirect.com

ScienceDirect

journal homepage: www.elsevier.com/locate/carbon

Accessing the local three-dimensional structure of carbon materials sensitive to an electron beam

J. Leschner [*], *J. Biskupek*, *A. Chuvilin* [1], *U. Kaiser*

Central Facility of Electron Microscopy, Ulm University, Albert-Einstein-Allee 11, D-89081 Ulm, Germany

ARTICLE INFO

Article history:
Received 11 April 2010
Accepted 6 July 2010
Available online 11 August 2010

ABSTRACT

The local three-dimensional (3D) structure of a broad variety of carbon materials cannot be accessed by electron tomography in the sub-nanometre range because the materials are beam-sensitive. We have modified existing tomographic approaches in bright-field transmission electron microscopy with respect to minimization of electron beam damage and optimized alignment. In the case of Vulcan XC72 carbon soot containing catalytically active platinum nanoparticles we demonstrate the applicability of our approach to study the internal arrangement of graphitic layers in 3D characterized by interplanar spacing, length and tortuosity. This approach will allow access to the 3D structure of other graphite-like carbon nanomaterials with sub-nanometre resolution.

© 2010 Elsevier Ltd. All rights reserved.

1. Introduction

Electron tomography in the transmission electron microscope (TEM) is the method of choice to reveal three-dimensional information in the nanometre regime in biology and materials science [1]. It is frequently used to clarify or provide new information on the structure of materials in three dimensions not accessible from two-dimensional observations. In addition a growing demand persists to obtain atomic resolution in all three dimensions, however, only a resolution of 1 nm^3 is achievable in electron tomography on a routine basis nowadays [2]. Atomic resolution tomography has been shown feasible on pure crystalline gold-nanoparticles incorporating a priori knowledge of regularly arranged atoms on the crystal grid [3]; however, this approach is not directly applicable to more complex sample morphologies like layered structures. Moreover, research in catalysis requires studies about the interaction of catalytically active nanoparticles with their support; e.g. carbon soot, due to its outstanding physicochemical nature preventing nanoparticles from agglomerating within operation cycles in fuel-cell applications [4,5]. The nature of the carbon allotropes diamond, graphite, nanotubes and fullerenes has been investigated by high-resolution (HR) TEM 2D imaging during the last decades (cf. reviews of Terrones and Terrones [6] and Harris [7]) and recently by aberration corrected HRTEM imaging with sub-Ångstrøm resolution (cf. for example [8–10]). Whereas graphite shows a layer spacing of 0.34 nm along the *c*-axis <0 0 2>, carbon soot consists of a much more irregular structure with different tortuosity and layer spacing [11,12]. Nanoparticles within carbon soot were already assessed with high angle annular dark-field (HAADF)–scanning (S)TEM tomography with respect to their shape, volume and distribution [13], but the internal three-dimensional structure of the support itself remained undiscovered so far. Its observation is hampered by its sensitivity to radiation damage caused by knock-on displacement, heating and/or chemical etching effects [14,15]. The knock-on displacement threshold for carbon lies between 27 and 95 kV [16], depending on the actual carbon configuration. To reveal the internal three-dimensional structure of e.g. carbon soot in its pristine stage, it is necessary, firstly, to operate the TEM below or near the corresponding knock-on damage

* *Corresponding author:* Fax: +49 731 50 22958.
E-mail address: jens.leschner@uni-ulm.de (J. Leschner).
[1] Present addresses: CIC nanoGUNE Consolider, Tolosa Hiribidea 76, E-20018 San Sebastian, Spain; IKERBASQUE, Basque Foundation for Science, Alameda Urquijo 36-5, E-48011 Bilbao, Spain.
0008-6223/$ - see front matter © 2010 Elsevier Ltd. All rights reserved.
doi:10.1016/j.carbon.2010.07.009

Author's personal copy

threshold, secondly, to work with an optimized electron dose to reduce all radiation damage processes as much as possible [17–19], and thirdly, to choose an operation mode allowing high-resolution imaging of the carbon soot while fulfilling the requirements for electron tomography.

Electron tomography itself requires, first, an acquisition method which provides a monotonic contrast mechanism relating signal intensity to sample thickness and elemental scattering cross-section (projection requirement) [20]; second, a high enough gain in signal-to-noise ratio with respect to the applied dose, and third, an alignment and reconstruction algorithm providing as much information from the only partly sampled 3D object inducing as less artefacts as possible.

In materials science electron tomography, HAADF–STEM is commonly used with its Z-contrast imaging capability for crystalline samples ensuring the projection requirement [21]. Atomic resolution in two-dimensional STEM imaging has been achieved by the decrease of probe size and the increase of beam current by aberration correction and enhanced electron sources, respectively; this ensures good signal-to-noise ratio [22], however, at the cost of strongly increased electron dose. Recently Buban et al. [23] have reported a roadmap to achieve two-dimensional, low-dose STEM imaging with similar conditions as TEM, but due to signal-to-noise limitation so far only for low-angle annular dark-field which shows less Z-contrast than necessary for sharp platinum on carbon [13]. On the contrary, ensuring the projection requirement, phase contrast imaging in TEM relates intensity linearly to the crystal potential for weak scattering materials and thin objects only [24,25]. Moreover, zero-loss energy filtered (EF)TEM extends the region of weak-phase approximation while improving contrast by removing inelastically scattered electrons. This results in good signal-to-noise conditions, which are preserved even for low-dose conditions [26]. Atomic resolution on electron beam-sensitive inorganic and organic test specimens has been shown recently by Evans et al. [27] with aberration corrected microscopes in phase contrast HRTEM imaging in combination with a low-dose approach. It can be concluded that zero-loss filtered aberration corrected HRTEM imaging combined with a low-dose protocol shall be promising for high-resolution electron tomography on beam-sensitive materials.

Low-dose protocols were originally established in the field of biological TEM tomography; here data collection for search, track, focus or exposure takes place at relatively low magnification ($\leq$30,000) and lower resolution with different settings for beam illumination, magnification and exposure time of the camera [28]. This ensures a cumulative dose of less than approximately $2{\cdot}10^3$ e^-/nm^2 for the entire tilt-series in biological electron tomography achieving a resolution of about 2 nm [29].

Generally, in order to obtain 3D tomographic data, the sample is imaged in 2D projection at various tilt angles. Imperfections in the acquired tilt series due to limited tilt angles, performance of the stage and projection system need to be corrected [30]. Back-projecting the tilt series into 3D space by Fourier-based or algebraic-based reconstruction techniques like ART are used to generate the desired 3D object [31].

Within this work methods from materials science and biological electron tomography are combined and extended to study the 3D nature of carbonaceous materials. In order to account for carbon knock-on damage and minimizing the overall beam damage, the accelerating voltage of the aberration corrected TEM was set to the commonly available option of 80 kV. We choose aberration-corrected zero-loss energy filtered HRTEM as imaging mode for data acquisition and establish corresponding low-dose imaging protocols. We intend to increase the resolution in the tomogram by refining existing alignment procedures as well as determining optimum reconstruction parameters.

Thus, we aim for revealing individual carbon layers in the interior of 3D carbon soot particles as well as layer configurations nearby catalytically active platinum nanoparticles on commercial Vulcan XC72. Our approach, moreover, should be applicable to other beam-sensitive carbon allotropes and may allow to reveal and quantify their internal three-dimensional structure.

2. Experimental

2.1. Material

For this study we used commercially available Vulcan XC72 with 20 wt.% Pt (ETeK, Inc.) containing platinum nanoparticles (atomic number $Z = 78$) supported on carbon soot. The powder was dispersed in ethanol by ultrasonic treatment and deposited on a lacey carbon film (Plano GmbH, Wetzlar, Germany).

2.2. Acquisition

The tomography tilt-series was obtained using a Titan 80–300 TEM (FEI, Netherlands) equipped with imaging C_S-corrector (CETCOR, CEOS GmbH, Germany) and post column energy filter (GIF, Tridiem 863, Gatan, US). The instrument was operated at 80 kV accelerating voltage. Special illumination conditions were used in order to optimize the damping envelope function of the microscope and to increase the information limit <0.12 nm [32]. Spherical aberration coefficient C_S was set to approximately +20 μm. Approximately −10 nm defocus were applied to obtain classical Scherzer conditions with dark atom contrast.

Images for rough tracking were acquired by pre-GIF CCD camera (1 k × 1 K 14 bit, type MSC794, Gatan, US) at magnification of ×48 K. Zero-loss filtered images (10 eV slit width) for tomographic series were acquired by post-filter CCD camera (2 K × 2 K 16 bit, type US1000, Gatan, US) without changing magnification. Assuming approximately ×15 post-magnification of the imaging filter, the effective magnification on the second CCD was around ×720 K, which corresponds to a field of view of 37×37 nm^2 for the investigated object (images are binned by 2 resulting in a sampling rate of 0.036 nm/px while resolving carbon and platinum reflexes up to 0.22 nm at ~0.33 × Nyquist to omit aliasing [33]). A single-tilt 2020 Advanced Tomography Holder (Fischione, US) was used.

In order to minimize the deposited dose, a number of precautions were taken: First, tracking, stigmation, focusing and acquisition were performed at different C2 condenser

Author's personal copy

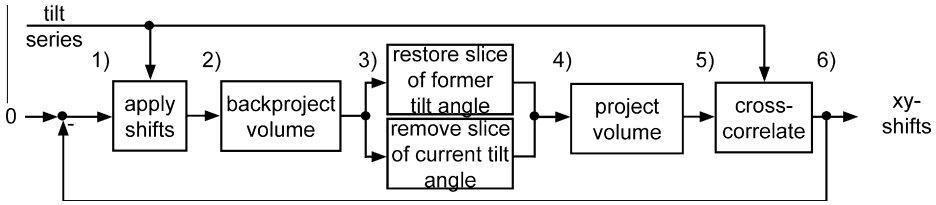

Fig. 1 – Sketch of the iterative alignment procedure producing x, y-shifts required for precise tilt-series alignment at each tilt angle: (1) apply the calculated x, y-shifts onto the tilt-series (at first iteration values are zero) (2) reconstruct pre-aligned tilt series obtaining 3D volume by weighted back-projection and remove negative intensities, (3) in order to improve convergence the original projection at the current tilt-angle is removed from 3D volume, (4) project volume at current tilt angle, (5) cross-correlate experimental image from tilt-series with projection and update alignment data, (6) proceed to step (1) with the updated x, y-shifts.

excitation (two-condenser lense mode in free control) ensuring the minimum required intensity. Second, a pre-specimen beam blanker was used in order to ensure specimen illumination only during camera exposition. Third, different cameras were used for tracking and acquisition, thus, eliminating the necessity for magnification change and additional tuning related to it. To automate this procedure and monitor the deposited dose at each intermediate step, a semi-automatic, user friendly utility was implemented based on the software interface TEMScripting (FEI, Netherlands).

2.3. *Alignment*

Following the standard procedure, first, cross-correlation alignment is applied for rough stacking of succeeding tilt images, and second, feature tracking for fine tuning, both carried out in the IMOD-package [34]. Due to partly occurring diffraction contrast, the images are pre-processed by a low-pass filter to enhance recognition of the nanoparticles, which have been used as fiducials for tracking. Thus, it is accounted for x, y-shifts, distortions, magnification changes, tilt-angles and an imprecise tilt-axis.

In order to overcome the necessity of fiducial tracking for fine alignment, an iterative self-consistent alignment strategy was established, which is based on weighted back-projection reconstruction and cross-correlation, resulting in x- and y-shifts (cf. Fig. 1). Final x-shifts account for tilt-axis inaccuracy in the x and z direction as well as arbitrary movements of the sample in x direction. Final y-shifts account only for the arbitrary movements during acquisition in y-direction. Both values are measured by cross-correlation with sub-pixel accuracy. A rotation of the tilt-axis in the x–y-plane is accounted for by manual adjustment by the method of "arcs of intensity" as described in [35] and for example available in Inspect3D (FEI, Netherlands).

2.4. *Reconstruction and quantification*

The algebraic reconstruction technique (ART) available from the open-source tomography package XMIPP [36] is used for reconstruction of the aligned series. The POCS (projection onto convex sets) approach for positivity constraint with n iterations and relaxation factor λ are chosen after optimization for best contrast of the reconstruction. For this purpose, a selected region of the tilt-series was reconstructed on a cluster computer system[2] by different (n, λ) sets and the contrast was measured from linescans across reconstructed carbon layers. The tilt series was pre-processed before reconstruction by background subtraction and afterwards inverted to relate the signal to high and the background to low intensity values. Fourier-ring-correlation (FRC) [37] and spectral-signal-to-noise-ratio (SSNR) [38], which are both available in XMIPP, are used to assess alignment improvements in the resulting 3D reconstruction. The reconstructed carbon layers were binarized within Avizo (TSG, Inc.) and measured with respect to layer distance, length and tortuosity (calculated by the Distance Metric as a ratio of layer path length and endpoint distance) by self-written code in MATLAB (Mathworks, Inc.).

3. Results and discussion

Although carbonaceous materials are beam-sensitive in general, the dose appropriate for an entire tilt series of at least 40 images depends on the actual configuration. While graphene would permit HRTEM exposures with a cumulative dose of $\sim 10^9$ e^-/nm^2, complex structures like soot require two order of magnitudes more strigent conditions. As illustrated in Fig. 2, carbon layers move half of their graphitic interplanar distance already at approximately 3.1×10^7 e^-/nm^2, which defines the dose limit for a tomographic tilt-series acquisition with 0.34 nm resolution. At approximately twice the cumulative dose the platinum nanoparticles change their position obviously by one third of their diameter, likewise defining the limit for a successful reconstruction for low-resolution nanoparticle investigation. Whereas individual carbon layer distances resist electron beam interactions, it is the weakest configuration within a soot particle which defines the success of the tilt-series acquisition (cf. Fig. 2, and "Supplementary Data"). Thus, the deposited dose has to be optimized and carefully distributed among the tilt-series by a low-dose protocol. Different doserates are predefined with respect to

[2] (http://www.bw-grid.de), Member of the German D-Grid initiative, funded by the Ministry of Education and Research (Bundesministerium für Bildung und Forschung) and the Ministry of Science, Research and the Arts Baden-Württemberg (Ministerium für Wissenschaft, Forschung und Kunst Baden-Württemberg).

Author's personal copy

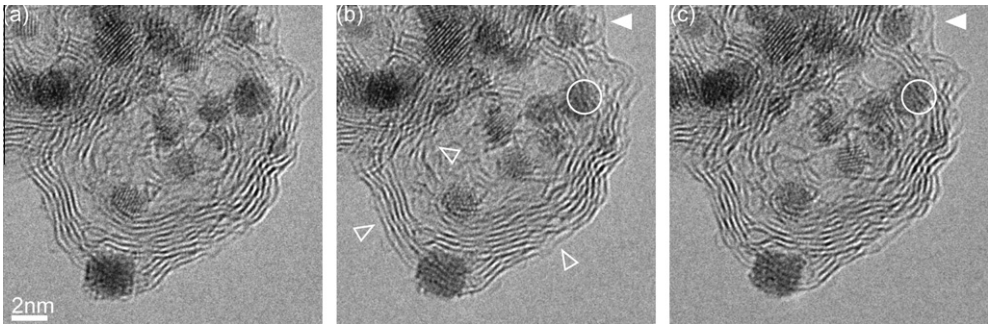

Fig. 2 – Time-series of a Vulcan XC72 carbon soot particle with platinum nanoparticles illustrating the dose limitation for a tomographic tilt-series (series is compensated for image shifts with the nanoparticle in the upper left corner as a reference point): (a) initial exposure serving as a reference; (b) after a cumulative dose of 3.1×10^7 e^-/nm^2 the carbon layer in the upper right corner has moved from its initial position (indicated by the filled white arrow) half of graphitic layer distance of 0.34 nm defining the dose limit for a tomographic reconstruction of carbon layers (unfilled white arrows indicate further positions at which layers are changed); (c) after a cumulative dose of 6.4×10^7 e^-/nm^2 the nanoparticle has moved one third of its diameter from its initial position (indicated by the white circle) besides the illustrated carbon layer(s) precluding a tomographic reconstruction of the nanoparticle either (carbon layers are black due to imaging near Scherzer conditions (positive C_S and underfocus)). The entire time series is available as a digital video in "Supplementary Data".

corresponding requisites for tracking (slight visibility of the field of view), stigmation (considerable SNR for the first Thon-ring in the FFT), focussing (slight visibility of carbon layers) and acquisition (resolution for the object) together with a beam blanker usage. This approach allows to acquire a tilt series of ±57° with a 3° tilt increment (46 images) for which the graphitic layers within the soot particle preserved their pristine configuration (cf. Fig. 3). In addition, it is possible to achieve a minimum dose of 1.7×10^7 e^-/nm^2 for acquisition and 1.3×10^7 e^-/nm^2 for tracking, stigmation, and focussing. Thus, the overall dose consumption enables to estimate the success of tilt-series acquisition on other structures in the future.

Standard alignment with platinum nanoparticles as fiducials resulted in remaining shifts observable in the series due to non-spherical, and moreover, overlapping particles, preventing high alignment accuracy. Thus, in order to achieve higher resolution in the alignment-prone x–z direction resulting in better distinguishable carbon layers, an iterative self-consistent alignment procedure was applied (cf. Fig. 3). The tilt-axis rotation in the x–y plane is adjusted manually by the help of nanoparticles up to an accuracy of ±0.5°. Deviations in experimental from true tilt-angles are not accounted for so far. Independent of the chosen alignment procedure, missing-wedge artefacts remain due to limited tilt-range and results in streaks at the top and bottom. Despite these limitations, the alignment could be improved by the iterative-self-consistent approach enhancing the FRC by a relative difference of 138% and the SSNR by 35% at the corresponding space frequency of 2.9 nm^{-1} (0.34 nm real space distance). Tilt dependent rotation and stretching of individual tilt images needs not to be accounted for as a small underfocus is required for aberration-corrected microscopy, which does not rotate the field of view, as well as our imposed dose limit for carbon layer resolution precludes sample shrinkage.

The aligned tilt-series was reconstructed by ART after the reconstruction parameters were optimized with respect to good convergence and contrast of carbon layers (set to $n = 40$ and $\lambda = 0.1$).

With this alignment procedure and optimized parameters we can clearly distinguish individual carbon layers of the carbon soot within the reconstruction, and thus, a resolution of at least 0.34 nm (typical graphite interplanar distance) has been achieved regularly (cf. Fig. 4). For the carbon layers the

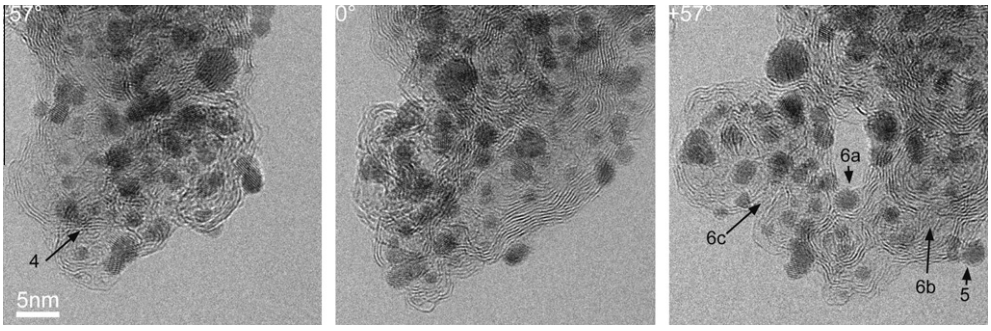

Fig. 3 – Images of zero-loss filtered bright-field TEM tilt-series of Vulcan XC72 carbon soot with platinum nanoparticles for a tilt-range of ±57° acquired with low-dose protocol achieving a total dose of 3.0×10^7 e^-/nm^2 (arrows indicate regions for Figs. 4–6). The entire tilt-series is available as a digital video in "Supplementary Data".

Author's personal copy

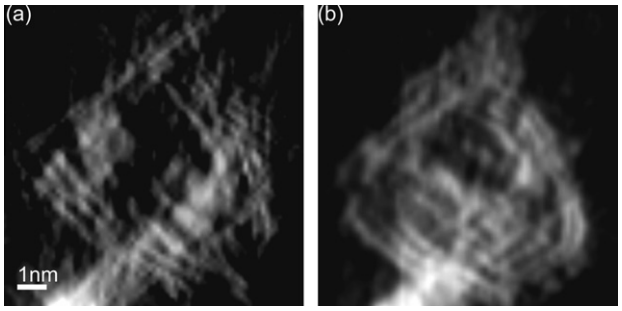

Fig. 4 – Comparison of different alignment schemes by reconstructed, alignment-prone *x*–*z* slices of the bottom tip of the soot particle in Fig. 2: (a) result of standard alignment with cross-correlation and feature tracking of low-pass filtered images by using platinum nanoparticles as fiducials within IMOD; (b) result of proposed iterative self-consistent alignment procedure shown in Fig. 1, correcting for *x*, *y*-shifts and revealing smooth and distinct carbon layers (in both cases, intensity was inverted in advance in order to relate carbon layers' (high) intensity for reconstruction to signal, thus, carbon layers are white now).

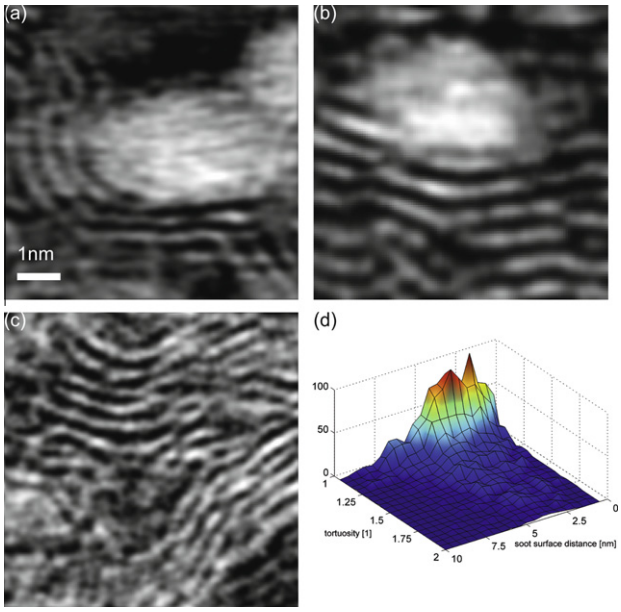

Fig. 6 – Slices of magnified regions of different carbon layer configurations within the soot: (a) regularly bended layers encompassing a platinum nanoparticle; (b) bended layers surrounding the particle in combination with curled ones resulting in occasionally larger inter-carbon spacing; (c) two regularly arranged regions merge while encompassing a region of higher disorder, and in (d) bivariate histogram correlating tortuosity of carbon layers with the 3D distance from the soot surface (carbon layers appear white).

projection requirement is fulfilled [39], whereas, crystalline platinum nanoparticles are affected by Bragg diffraction. The latter leads in some directions to an overlay in intensity with less contrast, though high enough to characterize surrounding carbon layers (cf. Fig. 4 at the lower left corner).

With this approach it is possible to study the carbon layer configuration around the catalytically active platinum particles and within the whole carbon soot. We found that the carbon layers are tightly surrounding the platinum nanoparticles either irregularly (cf. Fig. 5) or regularly (cf. Fig. 6a and b). The latter images depict that already several layers apart from the nanoparticles disordered layers are contributing to the overall soot structure. Carbon layers show a mean layer distance of (0.35 ± 0.06) nm, a mean layer length of (4.6 ± 2.7) nm, and a mean tortuosity of 1.20 ± 0.22 throughout the soot (values correspond to a measurement of 3400 carbon layers). Due to the accessible 3D information, these values can be correlated with the 3D position within the soot. A larger layer length (data not shown) and main contribution of low tortuosity near the surface (cf. Fig. 6d) indicates that the soot particle is hold together by long and straight carbon layers. Thus, it can be concluded that higher tortuosity is both related to areas like the soot tip where layers show a tortuosity of 1.2–1.4 as well as to parts more in the interior of the soot (cf. Fig. 6c), where for example two long-ranging regions merge while entangling a region with highly disordered carbon layers.

With this exemplified protocol, containing a low-dose protocol for high-resolution imaging and an iterative self-consistent alignment procedure, it is now possible to study structure related problems of electron beam-sensitive graphite-like carbon nanomaterials now in three dimensions.

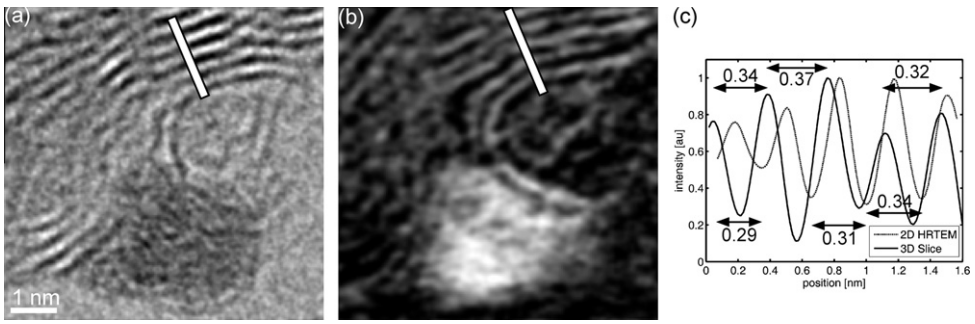

Fig. 5 – Estimating 3D resolution by a linescan across carbon layers with an assumed average spacing of 0.34 nm in the interior of the soot particle: (a) enlarged projection view from the 2D HRTEM tilt-series of Fig. 3 (carbon layers are black); (b) sliced section through the reconstructed volume at the same position as in (a) (carbon layers are white due to inversion prior to reconstruction); (c) the linescans for (a) and (b) show that at least 0.32 nm layer spacing are revealed by electron tomography and deviations from the average value within the volume can be measured.

Author's personal copy

4. Conclusion

A new protocol was established to access those carbon materials by electron tomography which are limited in resolution by the tolerable electron dose. Therefore, low-dose protocols with 80 kV spherical aberration-corrected HRTEM were combined with an iterative self-consistent alignment procedure to ensure accuracy requirements for sub-nanometre resolution in 3D. Different carbon layer configurations in carbon soot were revealed at a resolution of ~0.34 nm in 3D with a minimum electron dose of 3.0×10^7 e^-/nm^2 applied to the sample. Furthermore, carbon layer distance, length and tortuosity can now be quantified in 3D and correlated with the three-dimensional position within the soot. The presented method allows further insights into the formation process of carbon soot and into the influence of the carbon support to the catalytic activity of nanoparticles. Moreover, this minimum dose high-resolution electron tomography protocol should be applicable to study the structure of other carbonaceous material configurations in 3D. Future work will be addressed to develop strategies to further reduce the influence of beam damage which then may allow even higher resolution of the three-dimensional structure of beam-sensitive carbon materials.

Acknowledgment

We acknowledge financial support by the German Research Foundation DFG within the projects KA1295/7-1,2 and KA1295/10-1 "SALVE – Sub-Ångstrøm Low Voltage Electron microscopy" and of the Ministry of Science, Research and the Arts (MWK) of Baden-Württemberg within SALVE. We gratefully thank the bwGRiD project for the computational resources.

Appendix A. Supplementary data

Supplementary data associated with this article can be found, in the online version, at doi:10.1016/j.carbon.2010.07.009.

REFERENCES

[1] Möbus G, Inkson BJ. Nanoscale tomography in materials science. Mater Today 2007;10(12):18–25.
[2] Midgley PA, Dunin-Borkowski RE. Electron tomography and holography in materials science. Nat Mater 2009;8(4):271–80.
[3] Jinschek JR, Batenburg KJ, Calderon HA, Kilaas R, Radmilovic V, Kisielowski C. 3-D reconstruction of the atomic positions in a simulated gold nanocrystal based on discrete tomography: prospects of atomic resolution electron tomography. Ultramicroscopy 2008;108(6):589–604.
[4] Steele BCH, Heinzel A. Materials for fuel-cell technologies. Nature 2001;414(6861):345–51.
[5] Rolison DR. Catalytic nanoarchitectures – the importance of nothing and the unimportance of periodicity. Science 2003;299(5613):1698–701.
[6] Terrones M, Terrones H. The carbon nanocosmos: novel materials for the twenty-first century. Philos Trans R Soc Lond Ser A: Math Phys Eng Sci 2003;361(1813):2789–806.
[7] Harris PJF. New perspectives on the structure of graphitic carbons. Crit Rev Solid State Mater Sci 2005;30(4):235–53.
[8] Chuvilin A, Khlobystov AN, Obergfell D, Haluska M, Yang S, Roth S, et al. Observations of chemical reactions at the atomic scale: dynamics of metal-mediated fullerene coalescence and nanotube rupture. Angew Chem Int Ed 2010;49(1):193–6.
[9] Warner JH, Schäffel F, Zhong G, Rümmeli MH, Büchner B, Robertson J, et al. Investigating the diameter-dependent stability of single-walled carbon nanotubes. ACS Nano 2009;3(6):1557–63.
[10] Dahmen U, Erni R, Radmilovic V, Kisielowski C, Rossell M-D, Denes P. Background, status and future of the transmission electron aberration-corrected microscope project. Philos Trans R Soc Lond Ser A: Math Phys Eng Sci 2009;367(1903):3795–808.
[11] Vander Wal RL, Tomasek AJ, Pamphlet MI, Taylor CD, Thompson WK. Analysis of HRTEM images for carbon nanostructure quantification. J Nanopart Res 2004;6(6):555–68.
[12] Shim H-S, Hurt RH, Yang NYC. A methodology for analysis of 002 lattice fringe images and its application to combustion-derived carbons. Carbon 2000;38(1):29–45.
[13] Gontard LC, Dunin-Borkowski RE, Ozkaya D. Three-dimensional shapes and spatial distributions of Pt and PtCr catalyst nanoparticles on carbon black. J Microsc 2008;232(2):248–59.
[14] Banhart F. Irradiation effects in carbon nanostructures. Rep Prog Phys 1999;62(8):1181–221.
[15] Telling RH, Heggie MI. Radiation defects in graphite. Philos Mag 2007;87(31):4797–846.
[16] Kamimura O, Dobashi T, Kawahara K, Abe T, Gohara K. 10-kV diffractive imaging using newly developed electron diffraction microscope. Ultramicroscopy 2010;110(2):130–3.
[17] Egerton RF, Li P, Malac M. Radiation damage in the TEM and SEM. Micron 2004;35(6):399–409.
[18] Mølhave K, Gudnason SB, Pedersen AT, Clausen CH, Horsewell A, Bøggild P. Electron irradiation-induced destruction of carbon nanotubes in electron microscopes. Ultramicroscopy 2007;108(1):52–7.
[19] Kaiser U, Chuvilin A, Meyer J, Biskupek J. Microscopy at the bottom. In: Microscopy conference. Graz, Austria, 08/30-09/04; 2009. p. 1–6.
[20] Frank J. Electron tomography: three-dimensional imaging with the transmission electron microscope. New York: Plenum Press; 1992.
[21] Midgley PA, Weyland M, Thomas JM, Johnson BFG. Z-contrast tomography: a technique in three-dimensional nanostructural analysis based on Rutherford scattering. Chem Commun 2001(10):907–8.
[22] Krivanek OL, Nellist PD, Dellby N, Murfitt MF, Szilagyi Z. Towards sub-0.5 Å electron beams. Ultramicroscopy 2003;96(3–4):229–37.
[23] Buban JP, Ramasse Q, Gipson B, Browning ND, Stahlberg H. High-resolution low-dose scanning transmission electron microscopy. J Electron Microsc 2010;59(2):103–12.
[24] Ho MH, Jap BK, Glaeser RM. Validity domain of the weak-phase-object approximation for electron diffraction of thin protein crystals. Acta Crystallogr Sect A 1988;44(6):878–84.
[25] Bar Sadan M, Houben L, Wolf SG, Enyashin A, Seifert G, Tenne R, et al. Toward atomic-scale bright-field electron tomography for the study of fullerene-like nanostructures. Nano Lett 2008;8(3):891–6.
[26] Grimm R, Koster AJ, Ziese U, Typke D, Baumeister W. Zero-loss energy filtering under low-dose conditions using a post-column energy filter. J Microsc 1996;183(1):60–8.
[27] Evans JE, Hetherington C, Kirkland A, Chang L-Y, Stahlberg H, Browning N. Low-dose aberration corrected cryo-electron

Author's personal copy

microscopy of organic specimens. Ultramicroscopy 2008;108(12):1636–44.
[28] Koster AJ, Grimm R, Typke D, Hegerl R, Stoschek A, Walz J, et al. Perspectives of molecular and cellular electron tomography. J Struct Biol 1997;120(3):276–308.
[29] Conway JF, Trus BL, Booy FP, Newcomb WW, Brown JC, Steven AC. The effects of radiation damage on the structure of frozen hydrated HSV-1 capsids. J Struct Biol 1993;111(3):222–32.
[30] Mastronarde DN. Correction for non-perpendicularity of beam and tilt axis in tomographic reconstructions with the IMOD package. J Microsc 2008;230(2):212–7.
[31] Herman GT, Lent A, Rowland SW. ART: mathematics and applications: a report on the mathematical foundations and on the applicability to real data of the algebraic reconstruction techniques. J Theor Biol 1973;42(1):1–32.
[32] Meyer JC, Chuvilin A, Algara-Siller G, Biskupek J, Kaiser U. Selective sputtering and atomic resolution imaging of atomically thin boron nitride membranes. Nano Lett 2009;9(7):2683–9.
[33] Sherman MB, Brink J, Chiu W. Performance of a slow-scan CCD camera for macromolecular imaging in a 400 kV electron cryomicroscope. Micron 1996;27(2):129–39.
[34] Kremer JR, Mastronarde DN, McIntosh JR. Computer visualization of three-dimensional image data using IMOD. J Struct Biol 1996;116(1):71–6.
[35] Midgley PA, Weyland M. 3D electron microscopy in the physical sciences: the development of Z-contrast and EFTEM tomography. Ultramicroscopy 2003;96(3–4):413–31.
[36] Marabini R, Masegosa IM, San Martín MC, Marco S, Fernández JJ, de la Fraga LG, et al. Xmipp: an image processing package for electron microscopy. J Struct Biol 1996;116(1):237–40.
[37] Van Heel M. Similarity measures between images. Ultramicroscopy 1987;21(1):95–100.
[38] Unser M, Sorzano COS, Thevenaz P, Jonic S, El-Bez C, De Carlo S, et al. Spectral signal-to-noise ratio and resolution assessment of 3D reconstructions. J Struct Biol 2005;149(3):243–55.
[39] Götz A. Bestimmung optimaler Untersuchungsbedingungen für Elektronentomographie an Nanokohlenstoffobjekten. Diploma Thesis. Ulm Germany: Ulm University; 2010.